THE BELL SYSTEM
TECHNICAL JOURNAL

DEVOTED TO THE SCIENTIFIC AND ENGINEERING
ASPECTS OF ELECTRICAL COMMUNICATION

Volume 62 April 1983 Number 4, Part 1

Analysis of Thermally Induced Loss in Fiber-Optic Ribbons

By G. S. BROCKWAY* and M. R. SANTANA

(Manuscript received October 1, 1982)

In this paper, added loss during temperature cycling in a given ribboned fiber is shown to be caused by thermally induced axial compressive strain imparted to the fiber. A microbending-sensitivity parameter δ is introduced which reduces all loss-strain curves corresponding to different fibers to one characteristic master curve. Thermoviscoelasticity theory is used to calculate the time- and temperature-dependent compressive strain imparted to a ribboned fiber during a standard environmental cycle. Combining these analytical results with environmental data, the functional relationship between fiber-compressive strain and the added loss for a fiber of any given δ in an Adhesive-Sandwich Ribbon (ASR) with Urethane-Acrylate (UA) coated fibers has been determined. Using this analysis, the added loss for a UA ASR can now be predicted for any environmental cycle. The critical material properties that dominate the environmental performance of ASRs are the tape shrinkback at elevated temperatures and the product αEA of the coefficient α of thermal expansion, the time- and temperature-dependent relaxation modulus E, and the area A of the coating.

I. INTRODUCTION

Unless special precautions are taken, fiber-optic cables installed in the outside plant could experience temperatures ranging from −45°F

* Plastics Engineering Consultants, Inc., Lawrenceville, GA.

to +190°F. Thus, optical transmission loss resulting from this thermal history directly impacts the coating and ribbon choices for a particular system design. An understanding of the relationships among the thermally induced strains on the "ribboned" glass fibers, the resulting added transmission loss, and fiber parameters is crucial to properly evaluating candidate fiber-coating materials, ribbon structures, and/or ribbon-matrix materials. Moreover, it is desirable to be able to predict long-term behavior from short-term testing, thereby simplifying the environmental testing procedure.

The added loss in environmental testing is generally thought to be associated with the microbending of the axis of the fiber. Moreover, it has been shown by other investigators that when intimate contact is forced between a fiber and a microscopically rough surface, losses due to microbending can be substantial and are a function of the fiber geometric and optical parameters as well as the elastic modulus of the rough surface.[1,2] Therefore, thermally induced strains on the ribbon structure can indirectly result in added loss by increasing the contact forces between fibers. In addition, the sensitivity of a particular fiber to microbending loss is said to be associated with irregularities at the core-cladding interface, which may be due to core-diameter variations and/or refractive index variations.[3]

In this paper, a thermoviscoelastic analysis is used to compute the axial and transverse strains that are imparted to a fiber-optic ribbon when it is subjected to any given thermal cycle. This analysis shows that for the Bell System Adhesive-Sandwich-Ribbon[4] (ASR) construction with Urethane-Acrylate (UA) coated fibers, the transverse strain due to lowering the temperature results, contrary to one's expectation, in a reduction in the contact force between fibers. On the other hand, the resulting axial compressive strain evidently either increases this contact force or induces fiber buckling at the critical spatial wavelength, and thus creates added optical loss. Moreover, for a given ribboned fiber we establish herein the existence of a relationship between the environmental added loss and any measure of microbending sensitivity of the fiber. This equivalence enables us to predict the environmental performance of any ribboned fiber over a wide temperature-time span from data gathered over a relatively short time. In particular, the loss data collected from one excursion to −45°F can be combined with thermoviscoelastic data and analysis to predict the loss of any ribbon configuration with any choice of constituent materials, provided the tested fibers have a suitable range of microbending sensitivity.

II. ENVIRONMENTAL TEST PROCEDURE

The intent of environmental testing is to determine the effect of thermal exposure on the optical performance of fiber-optic ribbons. All

Table I—Environmental test cycle

Cycle Number	Exposure Temperature, T (°F)	Exposure Time, t (days)
I	75	2
	−45	2
	−15	2
	15	2
	75	2
	170	30
II	75	2
	−45	2
	−15	2
	15	2
	75	2
	190	34
III	75	2
	−45	2
	−15	2
	15	2
	75	2

the ribbons tested were placed in a 23-inch-diameter cardboard cylindrical container in a stem-pack fashion. The containers were then placed in a "walk-in" environmental chamber with both ends available for measuring purposes. Input and output array connectors[5] were fabricated to measure loss by the reference-fiber technique. Namely, the 0.63-μm loss of a fiber is obtained by taking the ratio of its output power to the average output power of ten reference fibers that are short enough to have negligible loss.

Table I is a summary of the environmental testing cycle used for this investigation. The loss of the ribboned fibers* was obtained at the end of each exposure. The change in loss for a typical ribboned fiber is plotted in Fig. 1 for each temperature in Cycles I, II, and III. The loss of the ribboned fibers increases with decreasing temperatures, the maximum loss occurring at the lowest temperature. As is evident in Fig. 1, the loss also increases with increasing cycle number. We subsequently show that this "pumping effect" is due to polyester-tape shrinkback† and stress relaxation effects during the high-temperature exposure between cycles.

It follows that for a 40-year design life, the worst-case environmental cycle would be a 40-year exposure at 190°F followed by a low-temperature exposure. This worst-case cycle is summarized in Table II. Note

* Fibers used in this study had cladding and core diameters of 110 and 55 μm, respectively.

† Shrinkback is the recovery of process-induced strains.

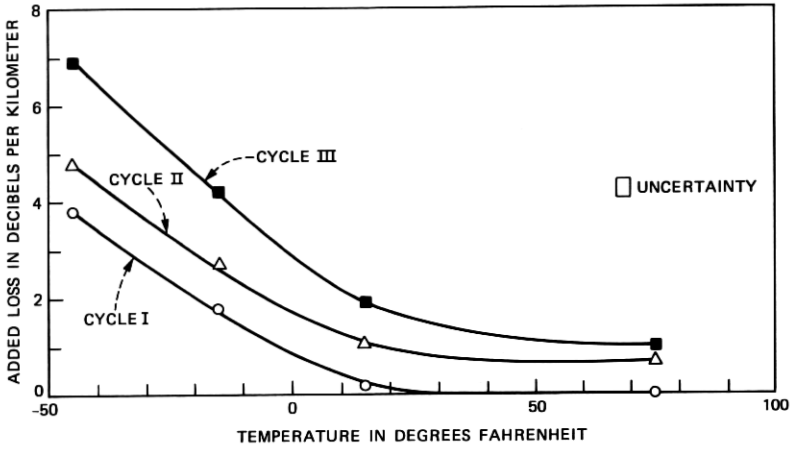

Fig. 1—Environmental added loss at 0.63 μm vs. temperature (UA-coated fiber, ASR construction).

Table II—Worst-case environmental cycle

Exposure temperature, T (°F)	Exposure Time, t (days)
190	14,610 (40 years)
75	2
−45	2
−15	2
15	2
75	2

that the cycle of Table II is not suggested for testing purposes but will only be used to predict the most pessimistic estimates of performance.

III. DUALITY BETWEEN MICROBENDING SENSITIVITY AND STRAIN

A convenient means for measuring the microbending sensitivity of different fibers is to determine the wavelength-independent loss coefficient[6] of the fiber when wound in several layers on a 6-inch-diameter reel under a tension fixed for all fibers. Let δ denote the wavelength-independent loss coefficient measured under these conditions. This method was contrived to produce artificially high losses, thereby magnifying the loss contribution due to microbending. Of course, the losses for these same fibers will be substantially smaller when measured in a stress-free configuration.

The added-loss response to a given cycle (see Fig. 1) is characteristic of all fibers of a single given δ (as defined above) in a given structure

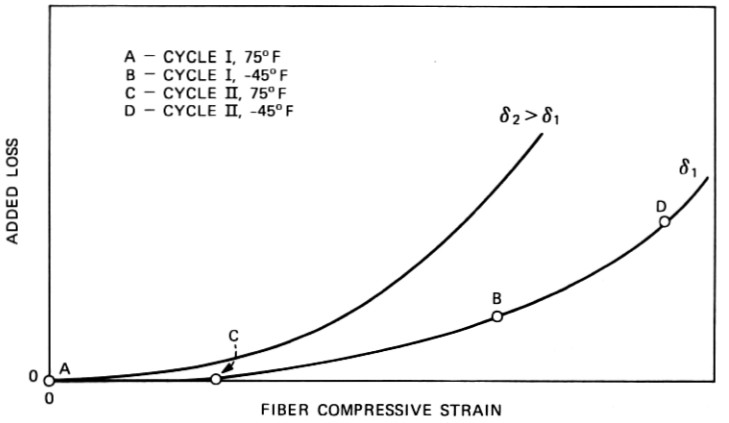

Fig. 2—Environmental added loss vs. fiber compressive strain.

but will change for fibers having different δ's. Moreover, examination of all the environmental data collected in this study indicates that the change in loss at a given point in any cycle increases with increasing δ.

As is well known, microbending loss occurs when the axis of a fiber is bent into a curve whose spectrum contains a certain critical frequency.[3] Transverse pressure against a fiber on a microscopically rough surface has been shown to introduce loss in this way.[1,2] However, in the case of environmentally induced loss in an ASR ribbon, it is shown in the Appendix that the *transverse* strain due to thermal contraction *reduces* the contact forces between fibers. Thus, the added-loss response of Fig. 1 must be due to another mechanism. The only reasonable possibility is that the compressive axial strain induces microbending loss through fiber buckling. This loss would occur if the fiber buckling were at the critical wavelength or if buckling increases the contact forces between the fiber and its surroundings. It is not our intent to identify which of these means dominates the behavior of the fiber but only to characterize its manifestations. In other words, we simply correlate the added loss with the compressive strain imparted to the fiber.

Both the added loss and compressive strain increase with decreasing temperature; their relationship* is shown schematically in Fig. 2. Here, the losses at 75°F and −45°F in Cycle I are denoted by *A* and *B*, respectively. After high-temperature exposure, the shrinkback of the polyester tape increases the strain on the fiber, so that *C* and *D*

* If strain and added loss monotonically increase with decreasing temperature, then it is easy to show that the added loss monotonically increases with increasing strain.

represent 75°F and −45°F in the second cycle. This explains the increased loss with each cycle that is evidenced in Fig. 1. This phenomenon has been observed consistently in all environmental testing and, as previously noted, is called the pumping effect.

Since the loss increases with increasing δ, the added-loss response to strain becomes steeper with increasing δ, as illustrated in Fig. 2. The effect of δ in this graph is obviously a contraction of the strain scale with increasing δ. As to whether this contraction is uniform or not is readily tested by plotting the loss versus logarithmic strain, where a uniform contraction would then appear as a horizontal, rigid translation of the added-loss curves with δ. As will be demonstrated in Section V, the loss-strain data may indeed be reduced in this fashion. Since the strain-scale contraction factor is a function of δ alone (the contraction is uniform), it creates a one-to-one correspondence (duality) between δ and compressive strain, changes in δ being equivalent to changes in strain. With this in mind, we proceed to a calculation of the axial strain in the environmental cycle.

IV. THERMOMECHANICAL ANALYSIS

This section is devoted to the summary of the formulas needed to calculate the axial strain history to which a fiber-optic ribbon is subjected during any environmental cycle. All of the plastics used in an ASR structure possess time- and temperature-dependent moduli, two examples of which are shown in Fig. 3. If the plastic is instantaneously strained, the stress required to sustain that strain relaxes with time according to the given curve. Notice that the relaxation that occurs in the UA modulus at 140°F in one hour takes more than 40 years at room temperature. The relaxation at −45°F is slower yet, so that the UA coating is as stiff as the polyester tape over significant time periods at these low temperatures.

On the other hand, the coefficients of thermal expansion of these plastics are constant with time provided the temperature changes do not encompass their glass transition temperatures, T_g. Even so, by virtue of the time dependence of the plastic moduli, the ribbon itself exhibits time- and temperature-dependent thermal expansion and contraction during the thermal cycle. This situation is depicted in Fig. 4. Since the expansion coefficients α_P of the plastics are much greater than that (α_G) for glass, the fibers restrain the contraction of the plastic, the net contraction $\alpha \Delta T$ of the ribbon being determined by equilibrium (force balance) in the structure. The relatively high short-time modulus of the plastic (see Fig. 3) causes the initial contraction (expansion) to be high. As the modulus of the plastic relaxes, the energy stored in the glass causes the ribbon to recover some of this high initial strain. Of course, the rate of this recovery depends on the temperature at which it occurs.

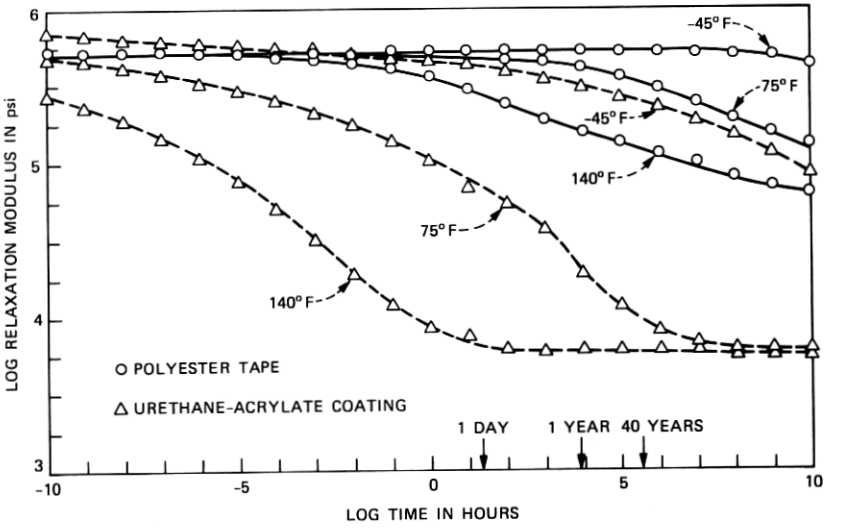

Fig. 3—Time dependence of moduli for ribbon constituents at various temperatures (generated by time-temperature superposition from data collected by R. P. DeFabritis).

The glass also resists shrinkback ϵ_S^{TA} of the polyester tape during exposure to elevated temperatures. If it were unrestrained, the tape would shrink back according to the results in Fig. 5. As illustrated in Fig. 6, the shrinkback ϵ_S that the ribbon experiences is much less than that of the free tape.

The compressive strain induced in the ribbon by its thermal contraction upon an excursion to −45°F is thus increased in each subsequent cycle by the shrinkback during the high-temperature exposure. We now proceed to a calculation of these strains.

4.1 Axial thermal expansion

If the plastic phases were considered to be elastic, the axial tensile modulus of a fiber-optic ribbon would be approximated well by the *rule of mixtures*

$$E_e = \frac{\sum_i E_i A_i}{\sum_i A_i}, \tag{1}$$

where E_i is the modulus of the ith constituent, A_i its area, and the summation is taken over all phases. In reality, (1) is a lower bound for the effective elastic modulus, being exact if all the constituents have the same Poisson's ratio.[7] Furthermore, eq. (1) can be derived in an elementary fashion by considering the equilibrium of the ribbon if one ignores Poisson's effect and assumes that all constituents are equally strained.

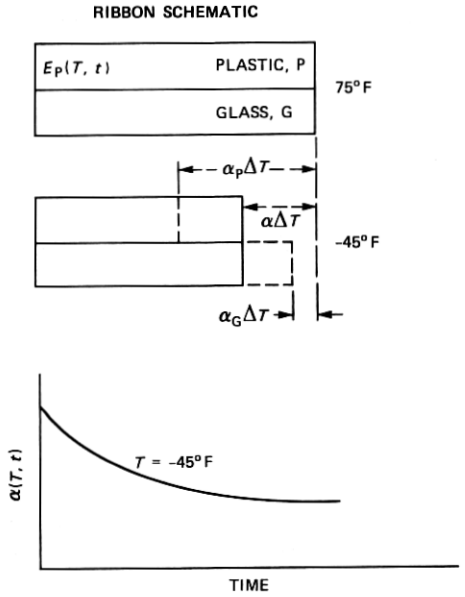

Fig. 4—Mechanics of ribbon thermal contraction.

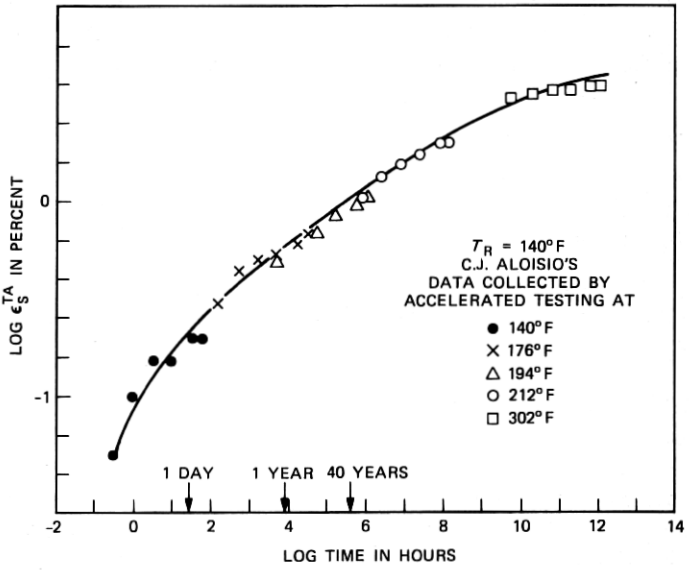

Fig. 5—Shrinkback strain vs. time for 3M No. 5 polyester tape.

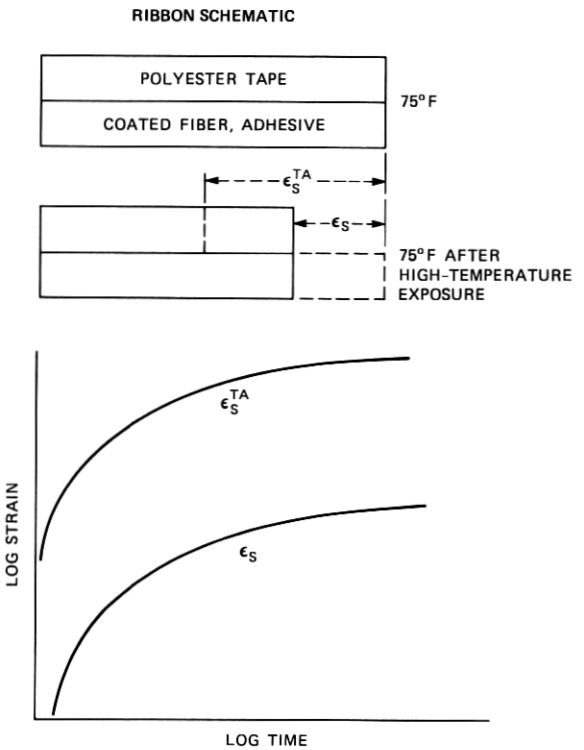

Fig. 6—Mechanics of ribbon shrinkback.

This same kind of elementary argument leads to the formula

$$\alpha_e = \frac{\sum_i \alpha_i E_i A_i}{\sum_i E_i A_i} \tag{2}$$

for the coefficient of thermal expansion of the ribbon, given elastic phases with moduli E_i, areas A_i and coefficients of thermal expansion α_i. Schapery has shown that (2) is exact if each phase has the same Poisson's ratio and is a very good approximation in any case.[7] These elastic results may be used to generate their viscoelastic counterparts. To see this, assume that all constituents obey constitutive equations of the *form*[8]

$$\sigma(t) = \int_0^t E(T(t), t - \tau)\dot{\epsilon}_\sigma(\tau)d\tau \tag{3}$$

$$E(T, t) = a_G(T)E(T_R, \xi), \qquad \xi = \int_0^t \frac{d\tau}{a_T(T(\tau))}$$

and

$$\epsilon_\sigma(t) = \epsilon(t) - \alpha[T(t) - T_0], \qquad T_0 = T(0), \tag{4}$$

where ϵ, σ, and $E(T, \cdot)$ are the strain, the stress and the relaxation modulus at temperature T, respectively. Here, a superposed dot on a function denotes differentiation with respect to its argument. On a log-log plot of modulus versus time, $\log a_G(T)$ and $\log a_T(T)$ represent, respectively, the vertical and horizontal distances that the curve for a temperature T must be translated to lay over that for the reference temperature T_R. All the materials considered here, including glass as a trivial case, conform to this hypothesis.

When (3) and (4) are met, it is readily shown that equation (1) continues to hold in the viscoelastic case, so that

$$E(T, t) = \frac{\sum_i E_i(T, t)A_i}{\sum_i A_i} \tag{5}$$

is exact (Poisson's effect being ignored). Moreover, as long as the curve of the logarithm of the modulus versus logarithmic time has small curvature, a good approximation to $\alpha(T, t)$ is provided by the so-called quasi-elastic approximation[8]

$$\alpha(T, t) = \frac{\sum_i \alpha_i E_i(T, t)A_i}{\sum_i E_i(T, t)A_i}. \tag{6}$$

The strain in the ribbon due to a temperature history T in the absence of stress is characterized by

$$\epsilon(t) = \int_0^t \alpha(T(t), t - \tau)\dot{T}(\tau)d\tau. \tag{7}$$

Notice that the ribbon has a time-dependent expansion coefficient even though we have supposed that the constituent plastics do not. This latter assumption is valid as long as the temperature excursion does not encompass the glass transition temperature T_g of any constituent. Equation (6) can easily be shown to continue to hold even if the constituents have time-dependent expansion coefficients. One need only replace each α_i by $\alpha_i(T, t)$. For the purposes of this investigation, it is sufficient to assume each α_i to be constant.

The data needed to calculate the effective modulus E and coefficient α of thermal expansion of the ribbon at −45°F and 75°F for a time of 10 hours is given in Table III. The geometric data of Table III was calculated using the nominal dimensions shown on the cross-sectional view of a typical ribbon in Fig. 7. Notice that although the glass makes far and away the most significant contribution to the stiffness of the

Table III—Geometric and material properties of ribbon constituents

	A (10^{-4} in.^{2})	α (10^{-5} °F^{-1})	Ten-Hour Modulus E(10^5 psi) −45°F	E 75°F	EA(10^2 lb) −45°F	EA 75°F	αEA (10^{-3}lb/°F) −45°F	αEA 75°F
3M No. 5 Polyester Tapes	3.00	1.06	5.27	4.67	1.58	1.40	1.67	1.48
3M No. 5 Acrylic Adhesive	3.60	7.72	0.00	0.00	0.00	0.00	0.00	0.00
Urethane-Acrylate Coatings	5.87	3.33	4.22	0.74	2.48	0.43	8.26	1.43
Glass Fibers	1.77	0.028	107	107	18.94	18.94	0.53	0.53
Total	14.24				23.00	20.77	10.46	3.44

Thus, eq. (6) $\rightarrow \alpha = \dfrac{\sum \alpha EA}{\sum EA} = \begin{matrix} 4.55 \times 10^{-6}\ °F^{-1} @ -45°F \\ 1.66 \times 10^{-6}\ °F^{-1} @ 75°F \end{matrix}$

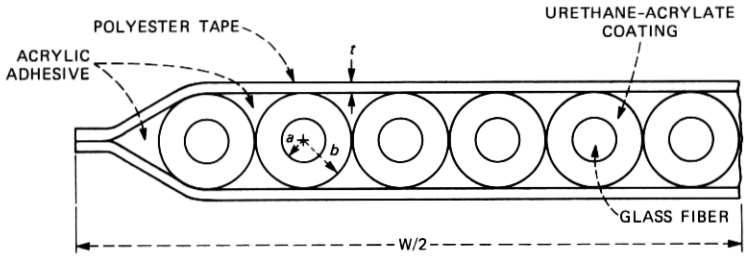

DIMENSIONS
a = 2.17 mils
b = 9.00 mils
t = 1.00 mil
w = 150 mils

Fig. 7—Cross section of a twelve-fiber ribbon.

ribbon, other constituents play a major role in the calculation of α. Indeed, at −45°F the αEA of the glass may well be neglected in comparison with that of the coating. At 75°F, on the other hand, the tape, coating and glass make comparable contributions to the effective thermal expansion coefficient.

In Fig. 8, α and E are plotted logarithmically against the logarithm of time at 75°F. It is evident that the change in α with respect to temperature and time is much more significant than the change in ribbon modulus. The coefficients of thermal expansion listed for each of the constituents in Table III are for temperatures below their respective glass transition temperatures, since our interests are in

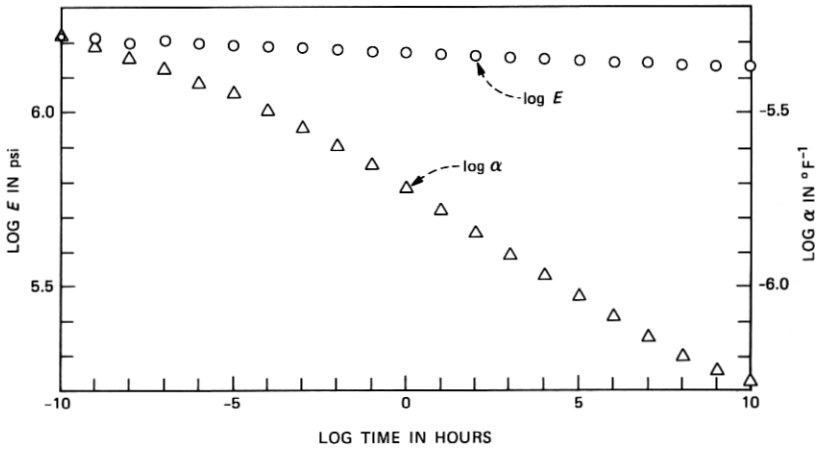

Fig. 8—Time dependence of the modulus and the coefficient of thermal expansion for the ribbon at 75°F (UA-coated fibers, ASR construction).

calculating the compressive strains imparted to the fiber during the low-temperature excursion.

If the ribbon is exposed to the temperature history

$$T(t) = T_0 + \sum_{k=1}^{n} (T_k - T_{k-1})H(t - t_k),\ H(t) = \begin{cases} 0 & t < 0 \\ 1 & t \geq 0 \end{cases} \tag{8}$$

$0 < t_1 < t_2 < \cdots < t_n < t$, the resulting strain history is

$$\epsilon(t) = \sum_{k=1}^{n} (T_k - T_{k-1})\alpha(T_n, t - t_k), \tag{9}$$

as found from substituting (8) into (7). Observe that eq. (9) contains all relaxation effects associated with the temperature history in (8).

4.2 Axial shrinkback

We now set out to calculate the shrinkback induced in the ribbon by the shrinkage of the polyester tape during high-temperature exposure. Denote by $\epsilon_S^{TA}(T_R, t)$ the shrinkback (see Fig. 5) the tape would experience in the time period $[0, t]$ at some reference temperature* T_R if it were unrestrained. At any other temperature T, the unrestrained shrinkback in the same time period would be

$$\epsilon_S^{TA}(T, t) = \epsilon_S^{TA}(T_R, t/a_T(T)), \tag{10}$$

where a_T is the temperature-dependent scale-contraction factor. If the tape is subjected to temperature T_1 for a time t_1 and then to T_2 for t_2, the total shrinkback would be

* $T_R = 60°$ in Fig. 5.

$$\epsilon_S^{TA}(T_R, t_1/a_T(T_1) + t_2/a_T(T_2)).$$

For the polyester tape used in the ASR construction, shrinkback is observable in the environmental cycle only during the high-temperature exposures, the time scales being much too long at the lower temperatures.

An analysis similar to that outlined in Section 4.1 for the time-dependent modulus and coefficient of thermal expansion of the ribbon can be used to obtain the approximate formula for the shrinkback strain of the ribbon ϵ_S.

$$\epsilon_S(t) \cong S(T, t)\epsilon_S^{TA}(t), \tag{11}$$

where

$$S(T, t) = \frac{E_{TA}(T, t)A_{TA}}{\sum_i E_i(T, t)A_i}. \tag{12}$$

A double logarithmic plot of the ribbon shrinkback function S as calculated from (12) is shown in Fig. 9 for $T = 140°F$. Observe that the shape of $\log S(T, \cdot)$ is very much like that of the logarithm of the polyester modulus in Fig. 3. The ribbon shrinkback during any high-temperature exposure can be calculated by substituting the appropriate mechanical and shrinkback data (e.g., Figs. 3 and 5) into eqs. (11) and (12). The error made in using eq. (11) at 140°F has been shown to decrease monotonically from 10 percent at two hours to 8.8 percent at ten hours. The approximation of eq. (11) increasingly improves as time goes on and as temperature increases. Since our interest is in times greater than forty-eight hours at temperatures over 170°F, (11) is quite acceptable.

4.3 Calculation of fiber compressive strains in the environmental test cycle

As discussed in Section III, a compressive strain applied to a riboned fiber induces added optical loss. This strain ϵ_F for the temperature history T [see eq. (8)] is given by

$$\epsilon_F(t) = \epsilon_R(t) - \alpha_F[T(t) - T_0], \tag{13}$$

where α_F is the linear coefficient of thermal expansion of the glass fiber and

$$\epsilon_R(t) = \epsilon(t) + \epsilon_S(t) \tag{14}$$

is the ribbon strain. In (14), ϵ is the strain due to the thermal contraction of the ribbon [eq. (9)], and ϵ_S is the ribbon shrinkback strain [eq. (11)].

Thermoviscoelastic data on each of the constituent materials were incorporated into computer-programmed versions of eqs. (6), (9), (11),

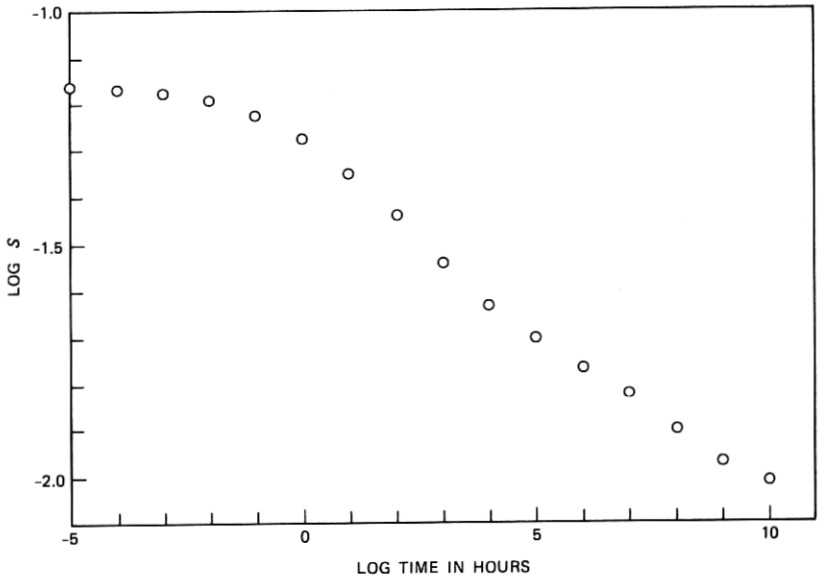

Fig. 9—Time dependence of ribbon-shrinkback function at 140°F (UA-coated fibers, ASR construction).

(12), and (13) to obtain the fiber strains on each excursion to −45°F. The results are plotted in Fig. 10.

V. THE MASTER CURVE FOR ADDED LOSS VERSUS COMPRESSIVE STRAIN

The purpose of this section is to construct the curve of added loss versus compressive strain (master curve) for a fiber having an arbitrary value of the microbending sensitivity parameter δ. This will be done by demonstrating that the effect of δ on the loss-strain curve is to uniformly contract the strain scale, which appears as a rigid shift (translation) of the curves with δ when the loss data are plotted against logarithmic strain. This master curve together with the δ-shift curve can then be used to predict the performance of any fiber (δ known) in any environmental cycle.

In Fig. 11, the environmental added-loss data for five fibers are plotted versus the logarithm of the axial compressive strain on the glass fiber as calculated in Section IV (Fig. 10). These data include all the measurements for Cycles I through III according to Table I. Neither of the points for 75°F in Cycle I appears in these figures because for the first the strain is zero and for the second it is tensile (negative), so that both logarithms are undefined.

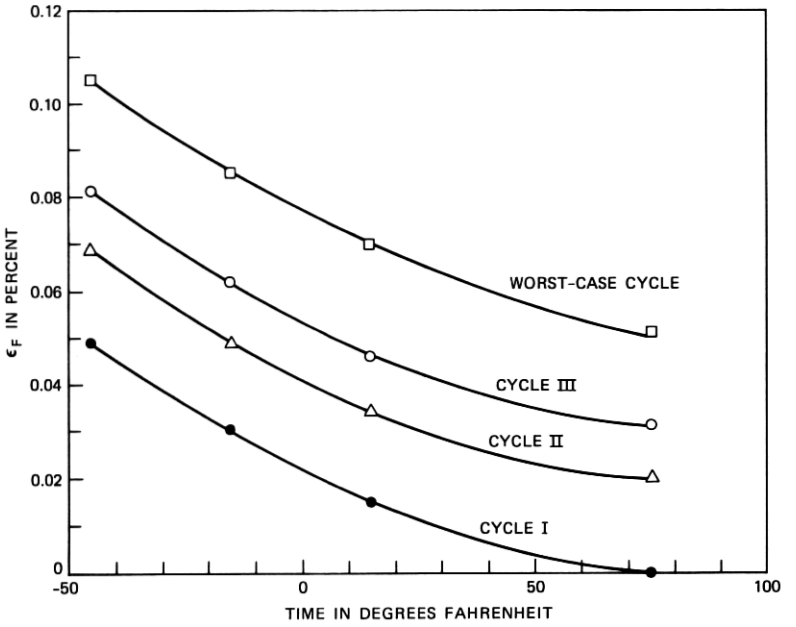

Fig. 10—Calculated fiber compressive strain vs. temperature in the environmental cycle (UA-coated fiber, ASR construction).

5.1 Shifting with δ to form the master curve

The plots in Fig. 11 were laid over one another and shifted horizontally by hand until they formed a single, smooth curve. The amount of shift log $a_\epsilon(\delta)$ required for each of the five values of δ is shown in Fig. 12 referenced to $\delta = 1.0$ dB/km. The linear, least-squares fit shown in Fig. 12 results in an excellent approximation of the shift data. For simplicity this linear approximation is used in the subsequent construction of the master curve.

The resulting master curve is shown in Fig. 13. The data points for the five different fibers are shown with different symbols on this plot. This master curve together with the δ-shift curve of Fig. 12 can be used to obtain the added-loss-versus-strain profile for a fiber of any given δ. A fourth-order polynomial has been fitted to the master curve data and is included in Fig. 13. Observe that the scatter about the best-fit polynomial is within the loss measurement uncertainty. Notice also that there is significant overlap in the data from fiber to fiber. On account of the functional relationship between a_ϵ and δ (illustrated in Fig. 12), we may view the master curve of Fig. 13 as added loss versus strain for a fixed value of δ or added loss versus δ for a fixed level of strain. This makes precise the δ-strain duality alluded to in Section III.

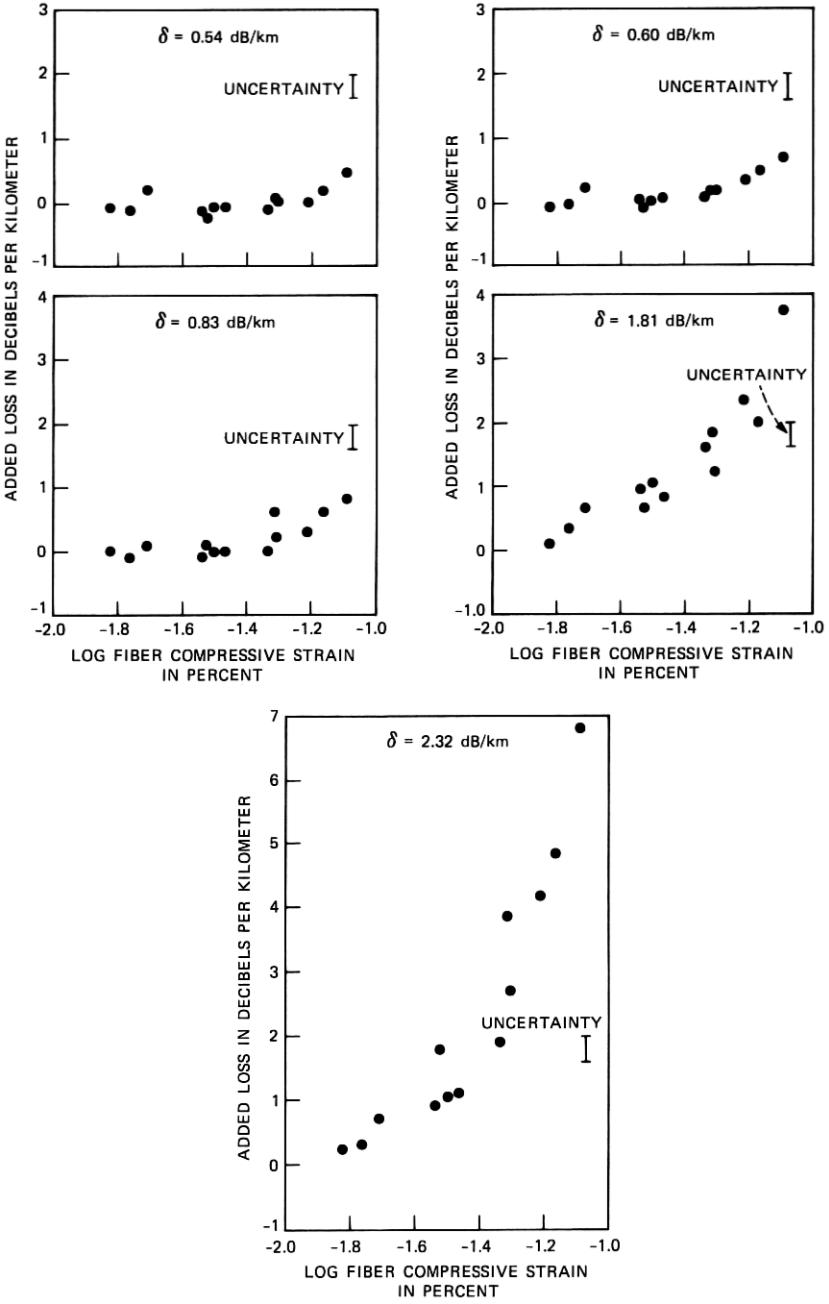

Fig. 11—Environmental added loss at 0.63 μm vs. calculated fiber strain in the environmental test (UA-coated fibers, ASR construction).

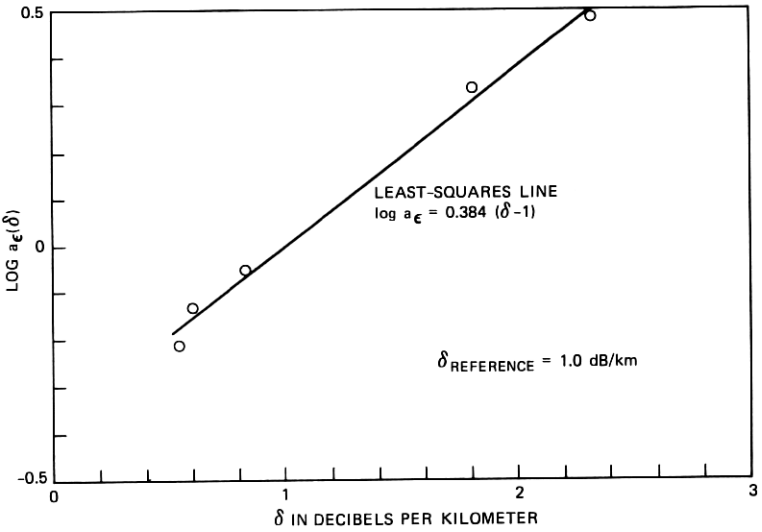

Fig. 12—Strain-scale-contraction factor vs. microbending sensitivity parameter δ (referenced to δ = 1.0 dB/km, UA-coated fibers, ASR construction).

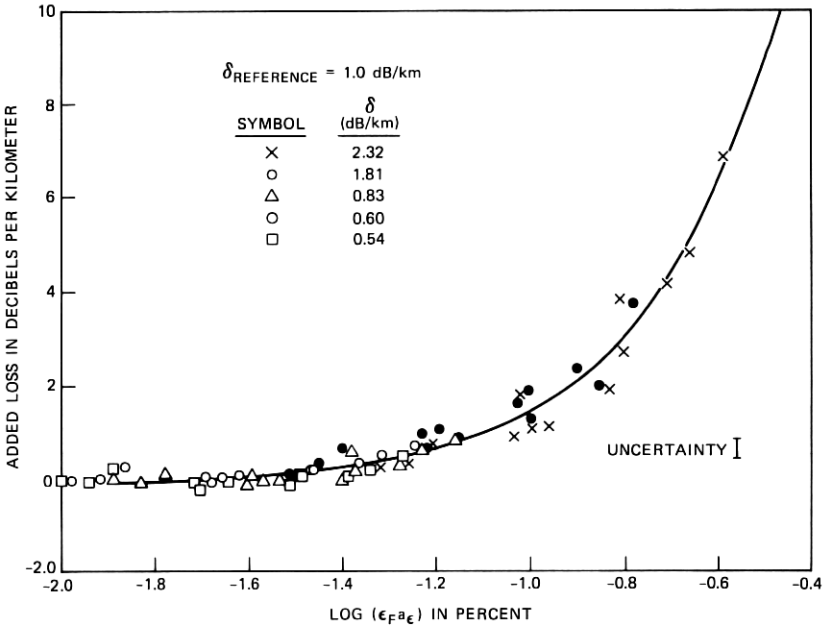

Fig. 13—Environmental added loss vs. δ-reduced fiber strain (referenced to δ = 1.0 dB/km, UA-coated fibers, ASR construction).

Although the master curve of Fig. 13 has been constructed from data collected in all three cycles, this was not necessary. Indeed, a polynomial fit through Cycle I is virtually indistinguishable from the one shown in Fig. 13. Thus, we are led to conclude that only one low-temperature excursion is necessary to complete an analysis of the type presented here, provided fibers having a suitable range of δ's are tested. This observation greatly simplifies the environmental-testing procedure for fiber-optic ribbons.

5.2 Prediction of loss in the worst-case cycle

We are now in a position to predict the behavior of a UA ASR in the worst-case environmental cycle. To do this we need only add to the strain associated with each temperature and time (see Fig. 10) the shift factor associated with the appropriate value of δ (see Fig. 12) for the fiber in question. The loss can then be read off the master curve (Fig. 13). For example, the strain ϵ_F in the worst-case cycle at $-45°$F obtained from Fig. 10 is 0.105%. The shift corresponding to a δ of 2.32 dB/km from the equation in Fig. 12 is $\log a_\epsilon(2.32) = 0.51$. Thus, the log of the δ-reduced strain [$\log \epsilon_F a_\epsilon(2.32)$], -0.47, yields an added loss of 9.8 dB/km from Fig. 13. This procedure was employed to generate the curves in Fig. 14 for the ribbon behavior in the worst-case cycle for different values of δ.

Notice for a δ of 2.32 dB/km in Fig. 14 that the loss in the worst-case cycle is much worse than that of Cycle III shown in Fig. 1. This

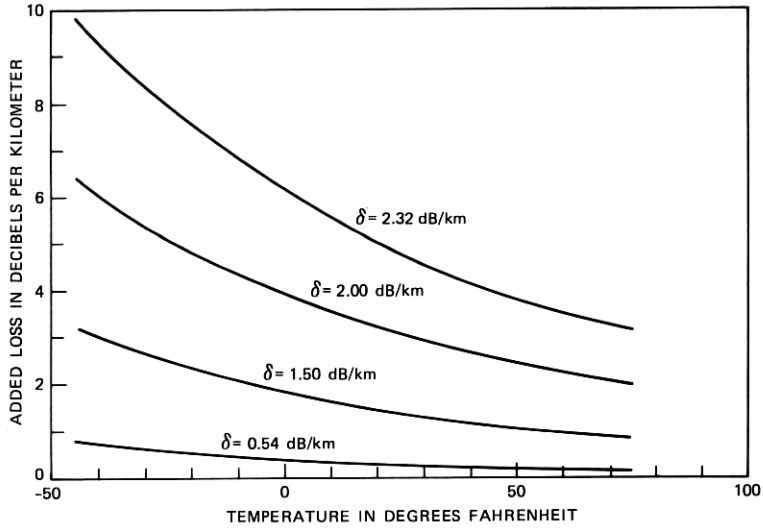

Fig. 14—Environmental added loss at 0.63 μm vs. temperature in the worst-case cycle (UA-coated fibers, ASR construction).

of course is the shrinkback effect previously discussed. Also, observe from comparing Figs. 11 and 14 that a fiber with $\delta = 0.54$ dB/km would meet a 0.5 dB/km added-loss criterion after Cycle III but not after the worst-case cycle. It is therefore clear that data sufficient to allow long-term predictions are essential to any meaningful ribbon evaluation. Finally, we remark that the added loss for a UA ASR can be predicted in the way demonstrated above for *any* environmental cycle provided one calculates the appropriate strain history by means of the formulas in Section IV.

VI. APPLICATIONS

6.1 A Criterion for coating/ribbon-structure comparisons

If one were to choose a ribbon-performance requirement of 1.0 dB/km in the worst-case cycle, then it is clear from Fig. 14 that an ASR made with a population of UA-coated fibers having high δ's would be unacceptable. The same structure manufactured with low-δ fibers would satisfy the requirement. Thus, one can easily err out of ignorance of the strong effect arising from the sensitivity of the fiber to microbending (as reflected in δ). Obviously, for a given performance requirement there is a maximum permissible δ-value, β. That is, if ribbons are manufactured from a fiber selection having δ's less than β, the given performance requirement will be met. Clearly then, it is not a question of whether the UA-ASR structure is acceptable or not, but rather how restrictive the value of β is. The parameter β is therefore an effective criterion for comparing various coating and ribbon-structure combinations.

To calculate this maximum permissible δ-value, β, for the UA ASR given a 1.0 dB/km added loss in the worst-case cycle, we enter into the master curve (Fig. 13) at a loss of 1.0 dB/km and read off the associated reduced strain

$$\log \epsilon_F a_\epsilon(\beta) = -1.09. \tag{15}$$

Next, introduce the equation for the δ-shift curve (Fig. 12),

$$\log a_\epsilon(\beta) = 0.384(\beta - 1)$$

into (15) to arrive at

$$\beta = 1 - \frac{1.09 + \log \epsilon_F}{0.384}. \tag{16}$$

Now the $-45°$F strain in the worst-case cycle is 0.105 percent, so that (16) yields

$$\beta = 0.7 \text{ dB/km}.$$

Similarly, for a performance requirement of 0.5 dB/km, one finds

$$\beta = 0.2 \text{ dB/km}.$$

Thus, UA-coated fibers selected with δ's less than β could be used in an ASR and satisfy the chosen performance requirement for a 40-year design life.

6.2 Critical material and geometric properties

The maximum permissible δ, β, can also be used to evaluate how material and geometric properties might be altered to improve environmental performance. It is obvious that a reduction in polyester-tape shrinkback would reduce environmental added loss. This is illustrated dramatically in Fig. 15, where the parameter β is plotted versus shrinkback normalized with respect to that of the present tape in the worst-case cycle (see Fig. 5). The two curves are for performance standards of 0.5 and 1.0 dB/km in the worst-case cycle. Notice that a 50-percent reduction increases β from 0.2 to 0.5 dB/km for the 0.5 dB/km performance requirement, while elimination of the shrinkback

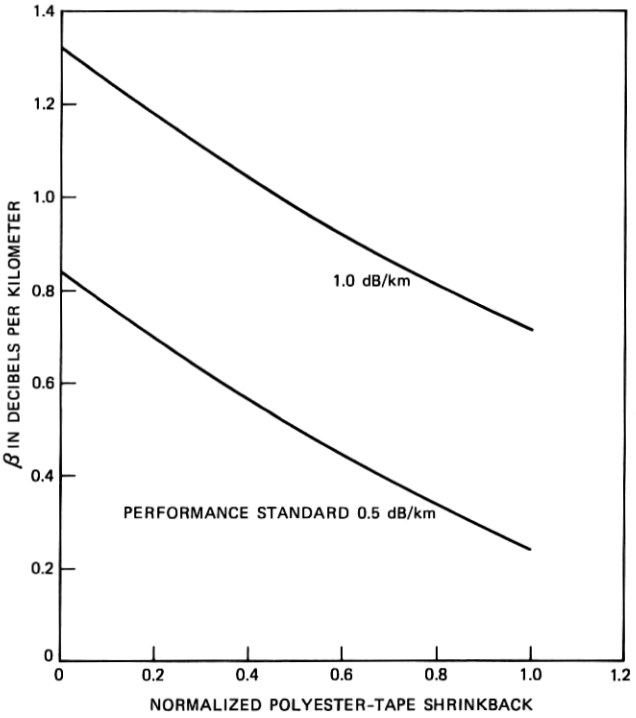

Fig. 15—Effect of shrinkback on the maximum permissible δ-value for the worst-case cycle (UA-coated fibers, ASR construction).

altogether increases β to 0.8 dB/km. Observe from eqs. (11) and (12) that the ribbon shrinkback is linear with respect to the area of the tape. Thus, Fig. 15 can also be viewed as a plot of β versus reduced area normalized to that of the present tape (see Table III).

A consideration of Table III reveals that reducing the αEA product of the coating will likewise diminish the strain on the fibers, since the coefficient of thermal expansion of the ribbon would then be reduced. The coefficients α of thermal expansion are essentially the same for all plastics though the moduli E can vary substantially from one material to another. Notice further that the area A of the coating is greater than that of any other ribbon constituent. As to whether this reduction in fiber strain is accompanied by an environmental performance improvement depends on the extent to which the added-loss-versus-compressive-strain master curve and its associated δ-shift characteristic are influenced by the changes adopted to reduce the fiber strain. Changing α of the coating has no effect on these curves while changing coating modulus E and/or the ribbon geometry may have a substantial effect. The variation in the shape of these curves with changes in these various parameters can be ascertained only by completing a characterization of the type carried out here for the UA ASR.

Figure 16 shows how strong an effect reducing thermal contraction can be when the change in the added-loss-reduced-strain characteristic is negligible. Here we have plotted β against the coated-fiber outer diameter holding the fiber diameter constant. Observe that if the outer diameter of the coated fiber is reduced from 9 to 6 mils the effect on β is bigger than the effect of a 50-percent reduction in tape shrinkback. Letting the coating thickness tend to zero results in an increase in β from 0.2 to 1.0 dB/km for the 0.5 dB/km performance requirement. If a 50-percent reduction in tape shrinkback is combined with a reduction in coated-fiber outer diameter to 6.5 mils, one can show that β increases from 0.2 to 0.9 dB/km. Finally, we remark that these same dramatic effects should occur with reductions in the coating modulus.

Other investigators have established that dual-coated fibers having a soft primary coating are less sensitive to microbending than fibers having a hard, single coating.[1] Such dual-coated fibers in an ASR should also behave well environmentally. To see this, consider a secondary coating of UA over silicone where the area of the UA skin is 1.56×10^{-5} in.^{2} Neglecting the stiffness of the silicone (it is three orders of magnitude smaller than that of UA), we obtained an effective single-coated UA diameter of 6.4 mils. The corresponding increase in β (Fig. 16) is from 0.2 to 0.6 dB/km for the 0.5 dB/km performance criterion. As previously mentioned these conclusions are predicated upon the assumption that the basic loss-strain characteristic of the ASR structure is relatively insensitive to changes in coating modulus.

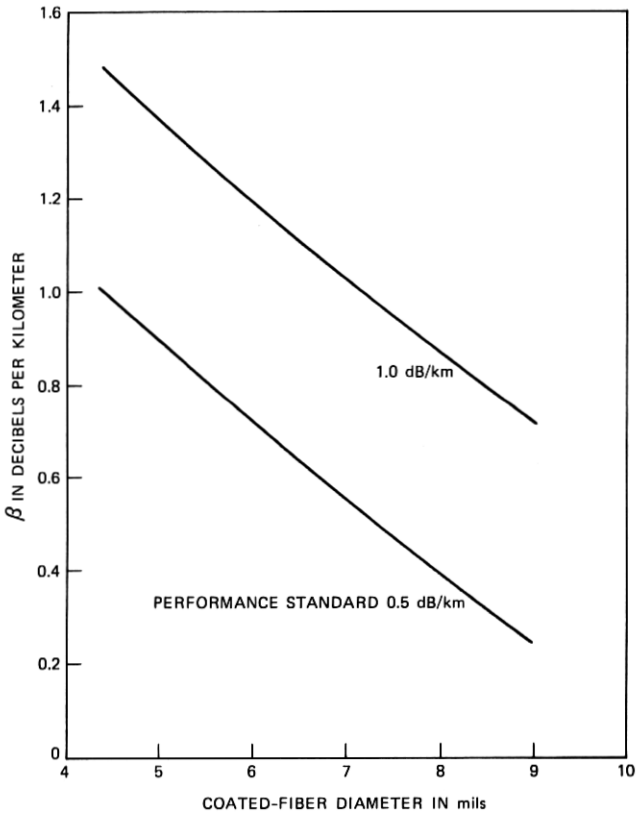

Fig. 16—Effect of coating thickness on the maximum permissible δ-value for the worst-case cycle (UA-coated fibers, ASR construction, fiber diameter = 4.33 mils).

VII. CONCLUSIONS AND RECOMMENDATIONS

We have shown that:

(*i*) Environmental added loss in an ASR is associated with axial compressive strain (not transverse strain) imparted to the fibers by thermal contraction of the ribbon in the low-temperature excursion and ribbon shrinkback together with relaxation during the high-temperature exposure.

(*ii*) There is a duality between a measure δ of the microbending sensitivity of a fiber and the fiber-compressive strain; viz., the effect of δ on the characteristic added-loss response to compressive strain is a uniform contraction of the strain scale.

(*iii*) Points (*i*) and (*ii*) above result in a master curve of environmental added loss versus δ-reduced fiber strain together with a plot of the strain-scale contraction factor versus δ-value. We are thus led to the algorithm depicted schematically in Fig. 17. Therefore, when

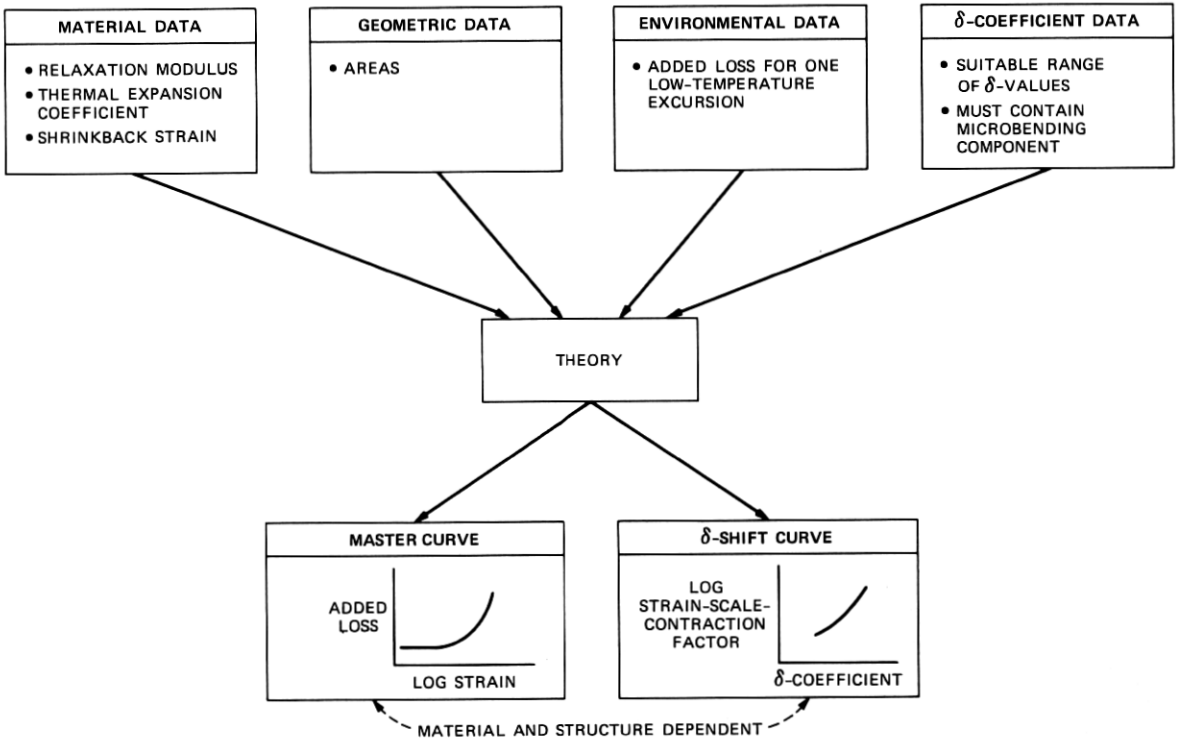

Fig. 17—Schematic of new environmental testing algorithm.

suitable material, geometric, environmental, and optical data are synthesized by way of our theory, we obtain a master curve and a δ-shift curve that are sufficient to predict the environmental added loss for the candidate ribbon configuration for any desired environmental cycle. Notice that this environmental-testing scheme eliminates the necessity for long-term testing, only one low-temperature excursion being required.

(*iv*) There is a maximum value of δ that a particular ribbon design can accommodate and still meet a given performance requirement. This maximum permissible δ-value is an excellent criterion for making coating/ribbon-structure comparisons.

By application of these techniques, we have found:

(*v*) The critical material and geometric parameters in ASR design are the shrinkback of the polyester tape and the product αEA of the coefficient α of thermal expansion, the time- and temperature-dependent relaxation modulus E, and the area A associated with the fiber coating.

(*vi*) Any method of reducing the αEA product of the coating such as introducing a soft, single coating or a dual system with a soft primary coating should improve environmental performance.

VIII. ACKNOWLEDGMENTS

This work was performed jointly with P. F. Mahr. The authors greatly appreciate the invaluable assistance provided by C. J. Aloisio, M. J. Buckler, R. P. DeFabritis, B. J. Overton, D. N. Ridgway, and C. R. Taylor all of Bell Laboratories in Atlanta, Georgia.

APPENDIX

Transverse Thermal Contraction of an Adhesive-Sandwich Ribbon

Consider a section of an ASR containing two coated fibers as shown in Fig. 18. If the temperature is instantaneously lowered by an amount

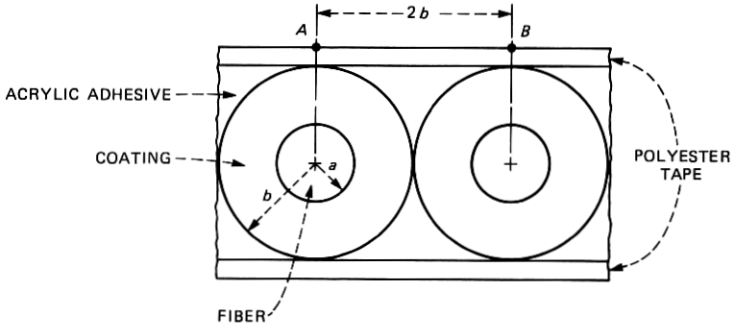

Fig. 18—Two-fiber portion of an ASR cross section prior to thermal contraction.

$|\Delta T|$ ($\Delta T < 0$) from the temperature T_0, the section AB of tape would have an unstressed length l_{TA} of

$$l_{TA} = 2b(1 + \alpha_{TA}\Delta T), \tag{17}$$

where b is the outer radius of the coated fiber and α_{TA} is the coefficient of transverse thermal expansion of the polyester tape.

A coated fiber would also shrink in diameter, the final radius b_f conforming to

$$b_f = b(1 + \alpha_*\Delta T), \tag{18}$$

where α_* is a number somewhere between the coefficients of thermal expansion of the glass and the plastic coating. To estimate α_* we appeal to linear thermoelasticity theory.

Denote by u and σ the radial displacement and stress fields (assumed axisymmetric) in the coating after the temperature is lowered. The stress field σ is to vanish at $r = b$, and it must match the stress in the glass fiber at $r = a$. The displacements must also match at this fiber-coating interface. Since the glass is many times stiffer than the plastic, we approximate the boundary conditions at $r = a$ by supposing the glass-coating interface to shrink with the glass coefficient of thermal expansion. Thus,

$$u(a) = a\alpha_F\Delta T, \sigma(b) = 0, \tag{19}$$

where α_F is the coefficient of thermal expansion of the glass fiber.

When the axisymmetric solution to the requisite field equations[9] is substituted into (19), a pair of simultaneous, linear algebraic equations for two unknown constants result. Solving these equations and doing some algebra, one deduces that

$$u(b) = \alpha_* b\Delta T, \tag{20}$$

where

$$\alpha_* = \frac{4}{3b^2/a^2 + 1}[(b^2/a^2 - 1)\alpha + \alpha_F] \tag{21}$$

when Poisson's ratio of the plastic is taken as 1/3.

For the case at hand, we use the values for a and b from the table in Fig. 7 and select α and α_F for the urethane-acrylate coating and the glass, respectively, from Table III. Substitution of these numbers into (21) gives

$$\alpha_* = 3.18 \times 10^{-5}\ {}^\circ F^{-1}, \tag{22}$$

which is 95 percent of the urethane-acrylate value.

If the final length l_{TA} of the tape segment is less than the final diameter $2b_f$ of the coated fiber, pressure will be created between the

fibers and microbending loss may result. Otherwise, the fibers will separate. Thus, the critical quantity is

$$d = l_{TA} - 2b_f. \tag{23}$$

Incorporating eqs. (17) and (18) into (23) results in

$$d = 2b\Delta T(\alpha_{TA} - \alpha_*). \tag{24}$$

For the case at hand $\alpha_{TA} < \alpha_*$ since the transverse thermal expansion coefficient for the tape is even less than the axial value reported in Table III. We thus conclude from (24) that d is positive (recall that $\Delta T < 0$).

Thus as the temperature is lowered the fibers separate and microbending loss from transverse contraction is therefore impossible. As the temperature is raised, however, the fibers obviously approach one another since at high temperatures α_{TA} is still less than α_*, but now $\Delta T > 0$. Moreover, there is transverse shrinkback at high temperatures. There is indeed environmental loss data which indicate increased loss at high temperatures.

REFERENCES

1. D. Gloge, "Optical-Fiber Packaging and its Influence on Fiber Straightness and Loss," B.S.T.J., *54*, No. 2 (February 1975), pp. 245–262.
2. W. B. Gardner, "Microbending Loss in Optical Fibers," B.S.T.J., *54*, No. 2 (February 1975), pp. 457–465.
3. D. Marcuse, "Losses and Impulse Response of a Parabolic Index Fiber With Random Bends," B.S.T.J., *52*, No. 8 (October 1973), pp. 1423–1437.
4. M. J. Saunders and W. L. Parham, "Adhesive Sandwich Optical Fiber Ribbons," B.S.T.J., *56*, No. 6 (July–August 1977), pp. 1013–1014.
5. C. M. Miller, "Fiber-Optic Array Splicing With Etched Silicon Chips," B.S.T.J., *57*, No. 1 (January, 1978), pp. 75–90.
6. K. Inada, "A New Graphical Method Relating to Optical Fiber Attenuation," Optics Commun., *19*, No. 3 (December 1976), pp. 437–438.
7. R. A. Schapery, "Thermal Expansion Coefficients of Composite Materials Based on Energy Principles," J. Composite Mater., *2* (July 1968), pp. 380–404.
8. R. A. Schapery, "Viscoelastic Behavior and Analysis of Composite Materials," *Composite Materials*, Vol. 2, Mechanics of Composite Materials, Ed. G. P. Sendeckyj, New York: Academic Press, 1974, pp. 85–168.
9. B. A. Boley and J. H. Weiner, *Theory of Thermal Stress*, New York: Wiley, 1960, p. 289.